

Geometric resonances in Bose–Einstein condensates with two- and three-body interactions

Hamid Al-Jibbouri¹, Ivana Vidanović^{2,3}, Antun Balaz̃^{2,4}
and Axel Pelster^{4,5}

¹ Institut für Theoretische Physik, Freie Universität Berlin, Arnimallee 14, D-14195 Berlin, Germany

² Scientific Computing Laboratory, Institute of Physics Belgrade, University of Belgrade, Pregrevica 118, 11080 Belgrade, Serbia

³ Institut für Theoretische Physik, Johann Wolfgang Goethe-Universität, D-60438 Frankfurt am Main, Germany

⁴ Hanse-Wissenschaftskolleg, Lehmkuhlenbusch 4, D-27733 Delmenhorst, Germany

⁵ Fachbereich Physik und Forschungszentrum OPTIMAS, Technische Universität Kaiserslautern, D-67663 Kaiserslautern, Germany

E-mail: antun@ipb.ac.rs

Received 9 October 2012, in final form 18 January 2013

Published 7 March 2013

Online at stacks.iop.org/JPhysB/46/065303

Abstract

We investigate geometric resonances in Bose–Einstein condensates by solving the underlying time-dependent Gross–Pitaevskii equation for systems with two- and three-body interactions in an axially symmetric harmonic trap. To this end, we use a recently developed analytical method (Vidanović *et al* 2011 *Phys. Rev. A* **84** 013618), based on both a perturbative expansion and a Poincaré–Lindstedt analysis of a Gaussian variational approach, as well as a detailed numerical study of a set of ordinary differential equations for variational parameters. By changing the anisotropy of the confining potential, we numerically observe and analytically describe strong nonlinear effects: shifts in the frequencies and mode coupling of collective modes, as well as resonances. Furthermore, we discuss in detail the stability of a Bose–Einstein condensate in the presence of an attractive two-body interaction and a repulsive three-body interaction. In particular, we show that a small repulsive three-body interaction is able to significantly extend the stability region of the condensate.

(Some figures may appear in colour only in the online journal)

1. Introduction

The experimental discovery of Bose–Einstein condensation [1–6] has instigated extensive experimental and theoretical studies of ultracold atoms and molecules. In particular, many experiments have focused on collective excitations of harmonically trapped Bose–Einstein condensates (BECs), as their frequencies can be measured to the order of a few per mill [7–10] and calculated analytically [11–17], and thus provide a reliable method for extracting ultracold system parameters.

A wide variety of interesting nonlinear phenomena are observed in collective excitations of BECs, including frequency shifts [18, 19], mode coupling [18, 20, 21], damping [9, 22], nonlinear interferometry [23], as well as collapse and

revival of oscillations [18, 24, 25]. The collective oscillation modes can be induced in a BEC by modulating the external potential trap [7, 8, 18, 26–39], the s-wave scattering length [19, 40–43] or three-body interactions [42, 44].

Resonant coupling between collective modes in a BEC was experimentally observed [20, 45], and it was shown that, when the parity quadrupole mode is excited by changing the trap anisotropy parameter above a certain value, it is possible to achieve an energy transfer between modes at a rate [21] which is comparable to the collective mode frequency. In [18], the frequency shift of collective modes due to the trap anisotropy in a generic axially symmetric geometry was studied, and it was shown that the collective modes exhibit a resonant

behaviour for specific values of the trap anisotropy, which are called geometric resonances, and that the strong effects can be observed even for oscillations of relatively small amplitude. The excitations and coupling of quadrupole and scissor modes in two-component BECs were investigated in [46]. Recently, also a coupling of the dipole, breathing and quadrupole modes close to a Feshbach resonance was analysed in [47].

In this paper, we study geometric resonances and resonant mode coupling in BECs with two- and three-body contact interactions. Theoretical studies of collective excitations are usually focused on two-body contact interactions due to the diluteness of quantum gases [10, 18–21, 41, 48]. However, the experimental progress with BECs in atomic waveguides and on the surface of atomic chips, which involve a strong increase in the density of BECs, also necessitates the study of three-body interactions [49–51]. Theoretical and experimental studies [49, 52, 53] for a BEC of ^{87}Rb atoms indicated that the real part of the three-body interaction term can be 10^3 – 10^4 times larger than the imaginary part. The imaginary part, which arises from three-body recombinations, limits the lifetime of the condensate. However, even for a small strength of the three-body interaction, the region of stability for the condensate can be extended considerably according to [54–57]. We study this in more detail and provide a phase diagram which demonstrates the significantly enhanced stability of BECs due to three-body interactions.

Due to the three-body interaction, the density profile [56], the excitation spectrum of the collective oscillations [59, 58] as well as the modulation instability of a trapped BEC [60] is modified. The effects of the three-body interaction were furthermore studied in ultracold bosonic atoms in an optical lattice [51, 61–68], BCS-BEC crossover [69], complex solitons BEC [70] and vortex BEC [71]. In addition, an extensive work was done on the study of cubic–quintic nonlinear equations, most notably in the context of nonlinear optics and superfluid helium. Even though these studies were done in uniform systems, many of the results are quite relevant for trapped systems as well. In particular, we mention studies of cavitation [72], droplets [73], as well as dynamics, solitary waves and vortex nucleation [74]. The transition temperature, the depletion of the condensate atoms and the collective excitations of a BEC with two- and three-body interactions in an anharmonic trap at finite temperature are studied in [75]. Reference [76] shows that the frequency of the collective excitation is also significantly affected by the strength of the three-body interaction and the anharmonicity of the potential. In [77], the authors investigated the collective excitations and the stability of a BEC in a one-dimensional trapping geometry for the case of repulsive or attractive three-body and repulsive two-body interactions.

Motivated by this, we study here the dynamics of the condensate with both two- and three-body contact interactions in general and its collective oscillation modes in particular by changing the geometry of the trapping potential. Within a Gaussian variational approach, the partial differential equation of Gross and Pitaevskii is transformed in section 2 into a set of ordinary differential equations for the condensate widths. We then discuss in detail in section 3 the resulting stability of the

condensate. First, we consider the case of an attractive two-body interaction and a vanishing three-body interaction, and afterwards the case of attractive two-body and repulsive three-body interactions. In section 4, we study geometric resonances and derive explicit analytic results for the frequency shifts for the case of an axially symmetric condensate based on a perturbative expansion and a Poincaré–Lindstedt method. This frequency shift is calculated for a quadrupole mode in subsection 4.1, for a breathing mode in subsection 4.2 and the derived analytical results are then compared with the results of numerical simulations in subsection 4.3. In that subsection, we also compare results of numerical simulations for radial and longitudinal condensate widths and the corresponding excitations spectra with the analytical results obtained using perturbation theory. Then, in section 5, we analyse the resonant mode coupling and the generation of second harmonics of the collective modes. Finally, in section 6 we summarize our findings and present our conclusions.

2. Variational approach

The dynamics of a Bose–Einstein-condensed gas in a trap at zero temperature is well described by the time-dependent Gross–Pitaevskii (GP) equation [76–81]. Usually, only two-body contact interactions are considered due to the diluteness of the gas. In this paper, however, we study systems where also three-body contact interactions have to be taken into account [82, 52]. In that case, the GP equation has the form

$$i\hbar \frac{\partial}{\partial t} \psi(\mathbf{r}, t) = \left[-\frac{\hbar^2}{2m} \Delta + V(\mathbf{r}) + g_2 N |\psi(\mathbf{r}, t)|^2 + g_3 N^2 |\psi(\mathbf{r}, t)|^4 \right] \psi(\mathbf{r}, t), \quad (1)$$

where $\psi(\mathbf{r}, t)$ denotes a condensate wavefunction normalized to unity and N is the total number of atoms in the condensate. On the right-hand side of the above equation, we have a kinetic energy term, an external axially symmetric harmonic trap potential $V(\mathbf{r}) = \frac{1}{2} m \omega_\rho^2 (\rho^2 + \lambda^2 z^2)$ with the anisotropy parameter $\lambda = \omega_z / \omega_\rho$, while the parameters g_2 and g_3 account for the strength of two-body and three-body contact interactions, respectively. The two-body interaction strength $g_2 = 4\pi \hbar^2 a / m$ is proportional to the s-wave scattering length a , where m denotes the mass of the corresponding atomic species.

The three-body interaction strength g_3 becomes important not only for large values of the s-wave scattering length, but also for small values of a close to the ideal gas regime. It is well known that the stability against the collapse of ^{85}Rb cannot be described by using only the two-body scattering [83]. The three-body scattering also plays an essential role in understanding the Efimov physics, where three bosons form a bound state [84, 85]. Braaten and Nieto [86] have used an effective field theory to calculate the strength of the three-body interaction, which effectively arises from the two-body interaction, and obtained the result $g_3(\kappa) = 384\pi (4\pi - 3\sqrt{3}) [\ln \kappa a + B] \hbar^2 a^4 / m$, where κ is an arbitrary wave number and B is a complex constant, both being suitably fixed in [86]. Thus, in general, the effective three-body coupling

strength represents a complex number, where its imaginary part describes recombination effects. However, its real part turns out to be much larger, and the fit to experimental data for ^{85}Rb and ^{87}Rb gives typical values for $\text{Re}(g_3)/\hbar$ of the order of 10^{-27} to $10^{-26} \text{ cm}^6 \text{ s}^{-1}$ [87, 75, 88].

Equation (1) can be cast into a variational problem, which corresponds to the extremization of the action defined by the Lagrangian $L(t) = \int \mathcal{L}(\mathbf{r}, t) \mathbf{dr}$, with the Lagrangian density

$$\mathcal{L}(\mathbf{r}, t) = \frac{i\hbar}{2} \left(\psi^* \frac{\partial \psi}{\partial t} - \psi \frac{\partial \psi^*}{\partial t} \right) - \frac{\hbar^2}{2m} |\nabla \psi|^2 - V(\mathbf{r}) |\psi|^2 - \frac{g_2 N}{2} |\psi|^4 - \frac{g_3 N^2}{3} |\psi|^6. \quad (2)$$

In order to analytically study the dynamics of BEC systems with two- and three-body interactions, we use the Gaussian variational ansatz, which was introduced in [15, 16]. For an axially symmetric trap, this time-dependent ansatz reads

$$\psi^G(\rho, z, t) = \mathcal{N}(t) \exp \left[-\frac{1}{2} \frac{\rho^2}{u_\rho(t)^2} + i\rho^2 \phi_\rho(t) \right] \times \exp \left[-\frac{1}{2} \frac{z^2}{u_z(t)^2} + iz^2 \phi_z(t) \right], \quad (3)$$

where $\mathcal{N}(t) = 1/\sqrt{\pi^{\frac{3}{2}} u_\rho^2(t) u_z(t)}$ is a normalization factor, while $u_\rho(t)$, $u_z(t)$, $\phi_z(t)$ and $\phi_\rho(t)$ are variational parameters, representing radial and axial condensate widths and the corresponding phases. The ansatz (3) describes dynamics of the condensate in terms of the time-dependent condensate widths and phases, while no centre-of-mass motion is considered here. A similar variational ansatz including the centre-of-mass motion has been studied in [89], and would be suitable to investigate how the centre-of-mass motion couples to the collective oscillation modes in the presence of three-body interactions.

If we insert the Gaussian ansatz (3) into the Lagrangian (2), we obtain the Lagrange function

$$L(t) = -\frac{\hbar}{2} (2\dot{\phi}_\rho u_\rho^2 + \dot{\phi}_z u_z^2) - \frac{m\omega_\rho^2}{2} \left(u_\rho^2 + \lambda^2 \frac{u_z^2}{2} \right) - \frac{\hbar^2}{2m} \left[\left(\frac{1}{u_\rho^4} + 4\phi_\rho^2 \right) u_\rho^2 + \left(\frac{1}{u_z^4} + 4\phi_z^2 \right) \frac{u_z^2}{2} \right] - \frac{g_2 N}{2(2\pi)^{3/2} u_\rho^2 u_z} - \frac{g_3 N^2}{9\sqrt{3}\pi^3 u_\rho^4 u_z^2}. \quad (4)$$

From the corresponding Euler–Lagrange equations, we obtain the equations of motion for all variational parameters. The phases ϕ_ρ and ϕ_z can be expressed explicitly in terms of first derivatives of the widths u_ρ and u_z according to

$$\phi_\rho = \frac{m\dot{u}_\rho}{2\hbar u_\rho}, \quad \phi_z = \frac{m\dot{u}_z}{2\hbar u_z}. \quad (5)$$

Inserting equations (5) into the Euler–Lagrange equations for the widths, we obtain the second-order differential equation for u_ρ and u_z . After introducing the dimensionless parameters

$$\tilde{\omega}_i = \omega_i/\omega_\rho, \quad \tilde{u}_i = u_i/\ell, \quad \tilde{t} = \omega_\rho t \quad (6)$$

with the oscillator length $\ell = \sqrt{\hbar/m\omega_\rho}$, we obtain a system of two second-order differential equations for u_ρ and u_z in the

dimensionless form

$$\ddot{u}_\rho + u_\rho - \frac{1}{u_\rho^3} - \frac{p}{u_\rho^3 u_z} - \frac{k}{u_\rho^5 u_z^2} = 0, \quad (7)$$

$$\ddot{u}_z + \lambda^2 u_z - \frac{1}{u_z^3} - \frac{p}{u_\rho^2 u_z^2} - \frac{k}{u_\rho^4 u_z^3} = 0, \quad (8)$$

where, for simplicity, we drop the tilde sign in the dimensionless widths. In the above equations,

$$p = \frac{g_2 N}{(2\pi)^{3/2} \hbar \omega_\rho \ell^3} = \sqrt{\frac{2}{\pi}} \frac{Na}{\ell} \quad (9)$$

denotes the dimensionless two-body interaction strength, while the parameter

$$k = \frac{4g_3 N^2}{9\sqrt{3}\pi^3 \hbar \omega_\rho \ell^6} \quad (10)$$

is the dimensionless three-body interaction strength, which can also be expressed in terms of p as

$$k = \frac{32}{9\sqrt{3}} \frac{g_3 \hbar \omega_\rho}{g_2^2} p^2. \quad (11)$$

For $N = 10^5$ atoms of ^{87}Rb [45, 51] in a trap with $\omega_\rho = 2\pi \times 112 \text{ Hz}$, the two-body interaction strength is $g_2 = 5\hbar \times 10^{-11} \text{ cm}^3 \text{ s}^{-1}$, yielding $p = 426$. The three-body interaction is of the order of $g_3 \approx \hbar \times 10^{-26} \text{ cm}^6 \text{ s}^{-1}$ [51], which gives the dimensionless three-body interaction value $k = 1050$.

Although the value of k is larger than that of p , the corresponding terms in equations (7) and (8), i.e. $k/u_\rho^5 u_z^2$ and $k/u_\rho^4 u_z^3$, are suppressed by the factor $u_\rho^2 u_z$ compared to the respective p -terms. The value of this factor can be estimated by taking into account the equilibrium positions $u_{\rho 0}$ and $u_{z 0}$, which are obtained by solving the stationary equations

$$u_{\rho 0} = \frac{1}{u_{\rho 0}^3} + \frac{p}{u_{\rho 0}^3 u_{z 0}} + \frac{k}{u_{\rho 0}^5 u_{z 0}^2}, \quad (12)$$

$$\lambda^2 u_{z 0} = \frac{1}{u_{z 0}^3} + \frac{p}{u_{\rho 0}^2 u_{z 0}^2} + \frac{k}{u_{\rho 0}^4 u_{z 0}^3}. \quad (13)$$

For the anisotropy $\lambda = 3/2$, one numerically obtains $u_{\rho 0} \approx 3.69$ and $u_{z 0} \approx 2.47$, yielding the value $u_{\rho 0}^2 u_{z 0} \approx 33.6$. This shows that the terms proportional to k have the effective coupling $k/33.6 \approx 31.2$, which makes them small corrections of the order of 7% to the leading two-body interaction terms. However, if the system exhibits resonances, this may no longer be true, and three-body interactions can play a significant role for the system dynamics. In this paper, we study geometric resonances, where it turns out to be necessary to take into account effects of three-body interactions. The s-wave scattering length can be tuned to any value, large or small, positive or negative, by applying an external magnetic field, using the Feshbach resonance technique [90, 91]. Therefore, in this paper we will consider a range of experimentally realistic values for dimensionless interaction strengths p and k .

Using the Gaussian approximation enables us to analytically estimate frequencies of the low-lying collective modes [15, 16, 19]. This is done by linearizing equations (7)

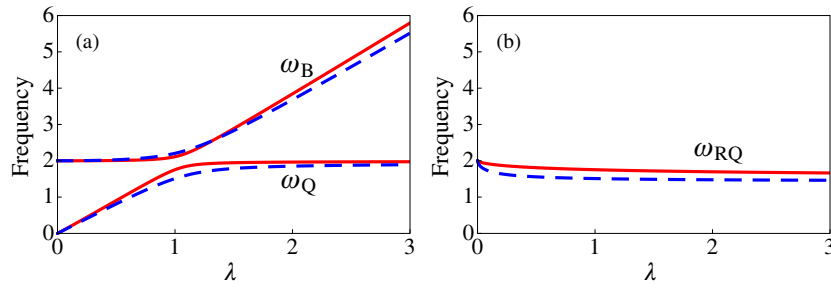


Figure 1. Frequencies (in units of ω_ρ) of collective oscillation modes for (a) breathing and quadrupole modes and (b) the radial quadrupole mode versus the trap aspect ratio λ for $p = 1, k = 0.001$ (solid red lines) and $p = 10, k = 0.1$ (dashed blue lines).

and (8) around the equilibrium positions. If we expand the condensate widths as $u_\rho(t) = u_{\rho 0} + \delta u_\rho(t)$ and $u_z(t) = u_{z 0} + \delta u_z(t)$, insert these expressions into the corresponding equations and expand them around the equilibrium widths by keeping only linear terms, we immediately obtain the frequencies of the breathing and the quadrupole modes,

$$\omega_{B,Q}^2 = \frac{m_1 + m_3 \pm \sqrt{(m_1 - m_3)^2 + 8m_2^2}}{2}, \quad (14)$$

where the abbreviations m_1, m_2 and m_3 are given by

$$\begin{aligned} m_1 &= 4 + \frac{2k}{u_{\rho 0}^6 u_{z 0}^2}, & m_2 &= \frac{p}{u_{\rho 0}^3 u_{z 0}^2} + \frac{2k}{u_{\rho 0}^5 u_{z 0}^3}, \\ m_3 &= 4\lambda^2 - \frac{p}{u_{\rho 0}^2 u_{z 0}^3}, \end{aligned} \quad (15)$$

and the corresponding breathing and quadrupole mode eigenvectors are given by

$$\mathbf{u}_{B,Q} = \frac{1}{\sqrt{m_2^2 + (\omega_{B,Q}^2 - m_1)^2}} \begin{pmatrix} m_2 \\ \omega_{B,Q}^2 - m_1 \end{pmatrix}. \quad (16)$$

The quadrupole mode has a lower frequency and is characterized by out-of phase radial and axial oscillations, while in-phase oscillations correspond to the breathing mode. Another low-lying collective excitation is the radial quadrupole mode, which is characterized by out-of-phase oscillations in the x and y directions, while in the z direction there are no oscillations. As this mode breaks the cylindrical symmetry, it can only be calculated by using the three-dimensional equations of motion. The frequency turns out to be

$$\omega_{RQ}^2 = 2 + \frac{2}{u_{\rho 0}^4}, \quad (17)$$

and the corresponding three-dimensional eigenvector is

$$\mathbf{u}_{RQ} = \frac{1}{\sqrt{2}} \begin{pmatrix} 1 \\ -1 \\ 0 \end{pmatrix}. \quad (18)$$

Figure 1 shows the frequencies of all collective oscillation modes as functions of the trap aspect ratio λ . We see that the collective mode frequencies depend relatively strongly on the trap anisotropy, whereas a variation of the dimensionless interaction strengths p and k yields only marginal changes.

3. Stability diagram

In this section, we discuss the stability of a BEC in the mean-field framework for systems with two- and three-body contact interaction in an axially symmetric harmonic trap. It is well known that BEC systems with an attractive two-body interaction are unstable against collapse above the critical number of atoms (i.e. for a sufficiently large negative value of p) in the condensate [80, 81]. For smaller numbers of atoms, the zero-point kinetic energy is able to counter the attractive inter-atomic interactions; however, when the number of atoms sufficiently increases, this is no longer possible, and the system collapses to the centre of the trapping potential.

We find that, for a pure two-body interaction, the condensate is stable only above a critical stability line $p_c(\lambda)$, while the presence of even a small repulsive three-body interaction leads to the stabilization of the condensate. On the other hand, we find that an attractive three-body interaction further destabilizes the condensate.

To study in detail the effects of the three-body interaction on the stability of BEC systems, we consider several cases of interest: repulsive and attractive pure two-body interactions, attractive two-body and repulsive three-body interactions, and attractive two- and three-body interactions. If the corresponding system of equations does (not) have positive and bounded solutions of equations (7) and (8) in the vicinity of positive equilibrium widths determined by equations (12) and (13), then the condensate is considered stable (unstable). This is equivalent to performing a linear stability analysis and determining the stability of positive equilibrium widths by examining frequencies of the corresponding collective oscillation modes (14) and (17). The solution is only stable if frequencies of all low-lying collective modes are found to be real; otherwise the solution is unstable.

For the case of a pure repulsive two-body interaction, we will immediately see that the condensate is always stable. For the case of an attractive two-body interaction, the situation is quite different: the above system of equations can have no equilibrium, or it could have up to three equilibrium solutions. The results of a detailed numerical analysis are summarized in figure 2.

The dashed red line in figure 2(a) represents the critical stability line as a function of the trap aspect ratio λ for a pure two-body interaction ($k = 0$). Below the critical stability line, there are no stable solutions and the system is unstable.

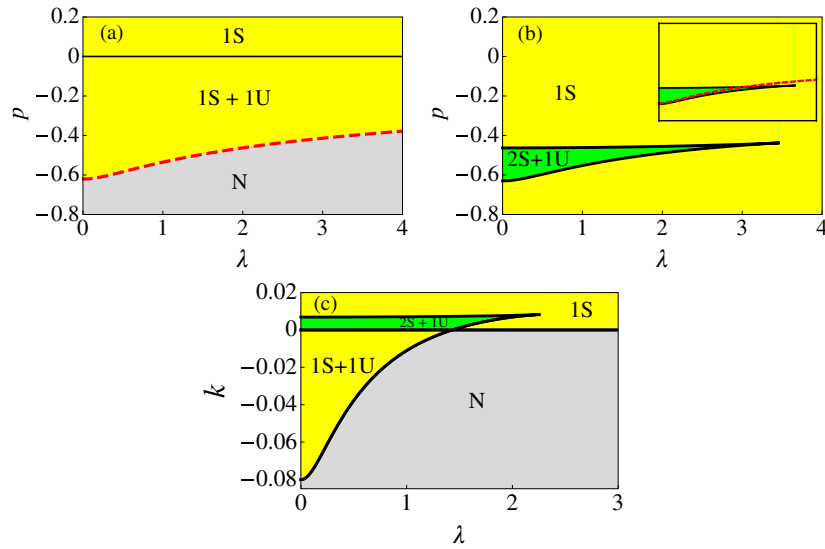


Figure 2. Stability diagram of a BEC as a function of a trap aspect ratio λ for different values of dimensionless two-body and three-body contact interaction strengths p and k . (a) λ - p stability diagram for $k = 0$, where the dashed red line represents the critical stability line, below which there are no solutions (N). Above this line, for $p < 0$, there is one stable and one unstable solution (1S+1U), while for $p \geq 0$ there is only one stable solution (1S). (b) λ - p stability diagram for $k = 0.005$, where two cases exist: the small region with two stable and one unstable solution (2S+1U), while otherwise only one stable solution exists (1S). For comparison, in the inset we combine the critical stability line for $k = 0$ with the stability diagram for $k = 0.005$. (c) λ - k stability diagram for $p = -0.5$. For $k \leq 0$, there are two regions: the one without solutions (N), and the one with one stable and one unstable solution (1S+1U). For $k > 0$, there are also two regions: the small region with two stable solutions and one unstable solution (2S+1U), while otherwise there is only one stable solution (1S). As we can see, a non-vanishing value of the three-body interaction k substantially enhances the stability of a condensate.

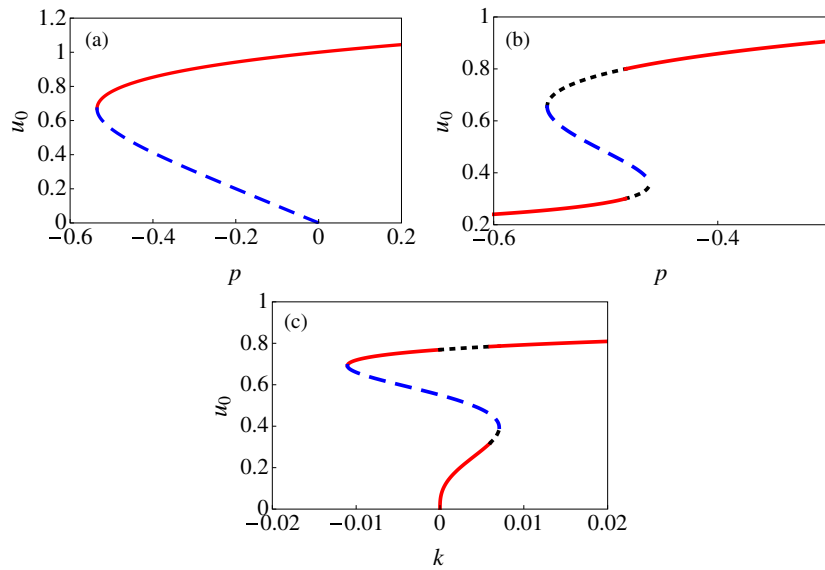


Figure 3. Condensate width $u_{\rho 0} = u_{z 0} = u_0$ for $\lambda = 1$ and (a) $k = 0$, as a function of p ; (b) $k = 0.005$, as a function of p ; (c) $p = -0.5$, as a function of k . The solid red lines represent the stable solution with minimal energy, the dotted black lines represent another stable solution and the dashed blue lines represent the unstable solution.

Above the critical stability line, the system has one stable and one unstable solution for an attractive two-body interaction ($p < 0$), and only one stable solution for a repulsive two-body interaction ($p \geq 0$). For $\lambda = 0$, which corresponds to the limit of a cigar-shaped condensate, we have the critical value of two-body interactions $p_c = -0.6204$, which coincides precisely with the value from [16]. For the isotropic case, when $\lambda = 1$, the critical value is $p_c = -0.535$, which again coincides with

the value from the literature [6, 16, 87, 57]. Figure 3(a) shows solutions for the isotropic condensate as a function of p .

Now, if we consider the case of an attractive two-body interaction and a small repulsive three-body interaction, then the results of the stability analysis are quite different. The system can either have one or three solutions, as shown in figure 2(b). The presence of a positive three-body interaction k , however small, leads to the existence of at least one stable

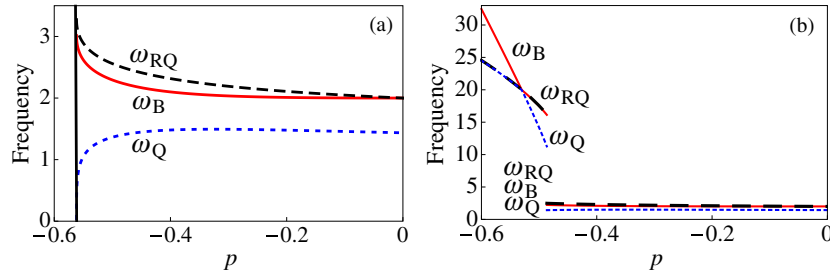


Figure 4. Frequencies (in units of ω_ρ) of low-lying collective excitation modes: breathing (B), radial quadrupole (RQ) and quadrupole (Q), as functions of an attractive two-body interaction p for the trap anisotropy $\lambda = 117/163$ and (a) $k = 0$, (b) $k = 0.005$.

solution in the whole range of values of λ and p . In the small area designated by 2S+1U in figure 2(b), two stable solutions and one unstable solution exist. Out of these two stable solutions, only the one with the minimal energy is physically relevant and could be realized in an experiment. Figure 3(b) shows solutions for $\lambda = 1, k = 0.005$ as a function of p . As we can see, a minimal-energy stable solution exists for any value of p . However, for large negative values of p this solution tends to zero, which practically represents a collapsed condensate. Therefore, although within the given mathematical model the condensate is always stable, physically this is valid only up to a critical number of atoms, which has to be determined by considering in detail the corresponding condensate density. However, as we can see from figure 3(b), the dependence $u_0(p)$ for large negative values of p is quite flat, which means that the stability region can be significantly extended in the presence of a small positive value of k compared to the case of pure two-body interaction.

We also analyse the stability of a BEC system as a function of the three-body interaction k . Figure 2(c) shows the corresponding stability diagram for an attractive two-body interaction $p = -0.5$. For a repulsive three-body interaction ($k > 0$), as expected, we see a small region with two stable solutions and one unstable solution (2S+1U), as well as a region with only one stable solution (1S), similar to figure 2(b). For an attractive three-body interaction ($k < 0$), the stability region with one stable and one unstable solution (1S+1U), which corresponds to the 1S+1U region in figure 2(a), gradually shrinks until it disappears as k becomes sufficiently negative. Therefore, we see that an attractive three-body interaction has the same destabilizing effect on a BEC as an attractive two-body interaction. This can also be seen in figure 3(c), where the stable minimal-energy solution for $p = -0.5$ exists only for a limited range of negative values of k .

To further illustrate the findings of the above stability analysis, we plot in figure 4 the frequencies of the low-lying collective excitation modes as functions of an attractive two-body interaction for the trap anisotropy $\lambda = 117/163$ [3]. Figure 4(a) corresponds to the case when three-body interactions are neglected, i.e. $k = 0$, and we can see that the condensate collapses for $p_c = -0.561$, when the expression for ω_Q^2 from equation (14) becomes negative. For a small repulsive three-body interaction $k = 0.005$, figure 4(b) shows the frequencies corresponding to stable minimum-energy solutions. From figure 3(b) we see that for $p_c = -0.486$

there is a jump from one to another solution branch due to the minimal energy condition, which is reflected in figure 4(b) by a corresponding jump in the frequencies of the collective modes.

4. Shifts in frequencies of collective modes

Close to geometric resonances, the nonlinear structure of the GP equation (1) leads to shifts in the frequencies of collective oscillation modes compared to the respective values in equation (14), which are calculated using a linear stability analysis. Here we apply the standard Poincaré–Lindstedt method [92–95, 19] in order to develop a perturbation theory and calculate these frequency shifts.

4.1. Quadrupole mode

We start with working out a perturbation theory for the BEC dynamic, which is based on the set of ordinary differential equations (7)–(8), by expanding the condensate widths in the series

$$u_\rho(t) = u_{\rho 0} + \varepsilon u_{\rho 1}(t) + \varepsilon^2 u_{\rho 2}(t) + \varepsilon^3 u_{\rho 3}(t) + \dots, \quad (19)$$

$$u_z(t) = u_{z 0} + \varepsilon u_{z 1}(t) + \varepsilon^2 u_{z 2}(t) + \varepsilon^3 u_{z 3}(t) + \dots, \quad (20)$$

where the smallness parameter ε stems from the respective initial conditions. Here we study the system dynamics with the initial conditions in the form

$$\mathbf{u}(0) = \mathbf{u}_0 + \varepsilon \mathbf{u}_Q, \quad \dot{\mathbf{u}}(0) = \mathbf{0}, \quad (21)$$

when the system is close to the equilibrium position \mathbf{u}_0 , and is perturbed in the direction of the quadrupole oscillation mode eigenvector \mathbf{u}_Q , determined by equation (16). By inserting expansions (19) and (20) into equations (7) and (8), we obtain the following system of linear differential equations:

$$\ddot{u}_{\rho n}(t) + m_1 u_{\rho n}(t) + m_2 u_{z n}(t) = \chi_{\rho n}(t), \quad (22)$$

$$\ddot{u}_{z n}(t) + 2m_2 u_{\rho n}(t) + m_3 u_{z n}(t) = \chi_{z n}(t), \quad (23)$$

where the index n takes integer values $n = 1, 2, 3, \dots$, and the quantities m_1, m_2 and m_3 are already defined by expressions (15). The functions $\chi_{\rho n}(t)$ and $\chi_{z n}(t)$ depend only on the solutions $u_{\rho i}(t)$ and $u_{z i}(t)$ of lower orders i , i.e. those corresponding to $i < n$. Therefore, the above system of equations can be solved hierarchically, and at each level n of this procedure, we use the initial conditions from equations (21).

In order to decouple the system of equations (22)–(23), we use the linear transformation

$$u_{\rho n}(t) = x_n(t) + y_n(t), \quad (24)$$

$$u_{zn}(t) = c_1 x_n(t) + c_2 y_n(t) \quad (25)$$

with the coefficients

$$c_{1,2} = \frac{m_3 - m_1 \mp \sqrt{(m_3 - m_1)^2 + 8m_2^2}}{2m_2}, \quad (26)$$

which leads to two independent linear second-order differential equations:

$$\ddot{x}_n(t) + \omega_Q^2 x_n(t) + \frac{c_2 \chi_{\rho n}(t) - \chi_{zn}(t)}{c_1 - c_2} = 0, \quad (27)$$

$$\ddot{y}_n(t) + \omega_B^2 y_n(t) + \frac{\chi_{zn}(t) - c_1 \chi_{\rho n}(t)}{c_1 - c_2} = 0. \quad (28)$$

From this we see that $x_n(t)$ and $y_n(t)$ correspond to quadrupole and breathing mode oscillations, respectively. Although the system is initially perturbed only in the direction of the quadrupole mode eigenvector, due to the nonlinearity of the system, the breathing mode is excited as well. The solutions of the above equations depend essentially on the nature of the inhomogeneous terms, which are given by polynomials of harmonic functions of $\omega_Q t$, $\omega_B t$ and their linear combinations $(k\omega_Q + m\omega_B)t$. Therefore, compared to linear systems, the important difference here is that higher harmonics and linear combinations of the modes emerge due to the structure of the GP equation.

A careful analysis also reveals the important conclusion that secular terms will start appearing at the level $n = 3$. As usual, they can be absorbed by a shift in the quadrupole mode frequency [19, 92–95]. At level $n = 3$, equations (22)–(23) can be written as

$$\ddot{\mathbf{u}}_3(t) + \mathcal{M}\mathbf{u}_3(t) + \mathbf{I}_{Q,3} \cos \omega_Q t + \dots = 0, \quad (29)$$

with the matrix \mathcal{M} defined as

$$\mathcal{M} = \begin{pmatrix} m_1 & m_2 \\ 2m_2 & m_3 \end{pmatrix}, \quad (30)$$

and the dots represent the inhomogeneous part of the equation, which does not contain linear terms proportional to harmonic functions in $\omega_Q t$. The expression for $\mathbf{I}_{Q,n}$ can be calculated systematically in the *Mathematica* software package [96].

The frequency shift of the quadrupole mode is found to be quadratic in ε :

$$\omega_Q(\varepsilon) = \omega_Q + \Delta\omega_Q = \omega_Q - \varepsilon^2 \frac{(\mathbf{u}_Q^L)^T \mathbf{I}_{Q,3}}{2\omega_Q}, \quad (31)$$

where \mathbf{u}_Q^L is the left-hand quadrupole mode eigenvector of the matrix \mathcal{M} . After a detailed calculation, the frequency shift of a quadrupole mode to lowest order in ε is found to be

$$\Delta\omega_Q = -\varepsilon^2 \frac{f_{Q,3}(\omega_Q, \omega_B, u_{\rho 0}, u_{z0}, p, k, \lambda)}{2\omega_Q(\omega_B - 2\omega_Q)(\omega_B + 2\omega_Q)}, \quad (32)$$

where $f_{Q,3}$ is a regular function, without poles for real values of its arguments. The above expression (32) has a pole for $\omega_B = 2\omega_Q$. Taking into account the fact that $\omega_Q < \omega_B$, as

we can see from equation (14) and figure 1, as well as the fact that collective frequencies depend on the trap aspect ratio λ , the condition $\omega_B = 2\omega_Q$ can, in principle, be satisfied. This is denoted as a geometric resonance, since it is obtained by simply tuning the geometry of the experiment through λ . Higher-order corrections to $\Delta\omega_Q$ in ε could, in principle, be obtained systematically by using the developed perturbation theory.

4.2. Breathing mode

In a similar manner, we also study the dynamics of a cylindrically symmetric BEC system when initially only the breathing mode is excited,

$$\mathbf{u}(0) = \mathbf{u}_0 + \varepsilon \mathbf{u}_B, \quad \dot{\mathbf{u}}(0) = \mathbf{0}. \quad (33)$$

Applying again the Poincaré–Lindstedt perturbation theory, we calculate the breathing mode frequency shift,

$$\omega_B(\varepsilon) = \omega_B + \Delta\omega_B = \omega_B - \varepsilon^2 \frac{(\mathbf{u}_B^L)^T \mathbf{I}_{B,3}}{2\omega_B}, \quad (34)$$

where again the expression $(\mathbf{u}_B^L)^T \mathbf{I}_{B,3}$ is calculated in *Mathematica*. In this way, we finally yield the following analytic formula for the frequency shift of the breathing mode

$$\Delta\omega_B = -\varepsilon^2 \frac{f_{B,3}(\omega_Q, \omega_B, u_{\rho 0}, u_{z0}, p, k, \lambda)}{2\omega_B(2\omega_B - \omega_Q)(2\omega_B + \omega_Q)}, \quad (35)$$

where the function $f_{B,3}$ is a regular function of its arguments. Naively looking at this expression, one would say that it exhibits a pole for $2\omega_B = \omega_Q$. However, from equation (14) and figure 1 we see that $\omega_Q < \omega_B$, and, therefore, the condition $2\omega_B = \omega_Q$ is never satisfied. In the following subsection, we numerically demonstrate that a geometric resonance does not occur, and verify the analytical result for the frequency shift of the breathing mode.

4.3. Comparison with numerical results

In order to verify our analytical results, we perform high-precision numerical simulations [97–105]. At first we focus on a description of the BEC dynamics, and compare our analytical results for the radial and longitudinal widths of the condensate obtained perturbatively to the direct numerical solutions of equations (7)–(8). To this end, we consider a BEC in the initial state corresponding to the perturbed equilibrium position, where the small perturbation is proportional to the eigenvector of the quadrupole mode according to equations (21). Examples of the condensate dynamics are shown in figure 5 for a pure two-body interaction $p = 1$, $k = 0$ with $\varepsilon = 0.1$, and in figure 6 for $p = 1$, $k = 0.001$, $\varepsilon = 0.1$.

In both figures, we plot analytical and numerical solutions for u_ρ and u_z as functions of the dimensionless time parameter $\omega_\rho t$ for different values of the trap aspect ratio λ . Analytical solutions are calculated using the third-order perturbation theory developed in subsection 4.1. We can see in figure 5 that the agreement is excellent, not only for the non-resonant value of the trap aspect ratio $\lambda = 2.3$ (top panels), but also for $\lambda = 0.55$ (bottom panels), which is close to a geometric resonance, as we will see later in figure 8(a). For

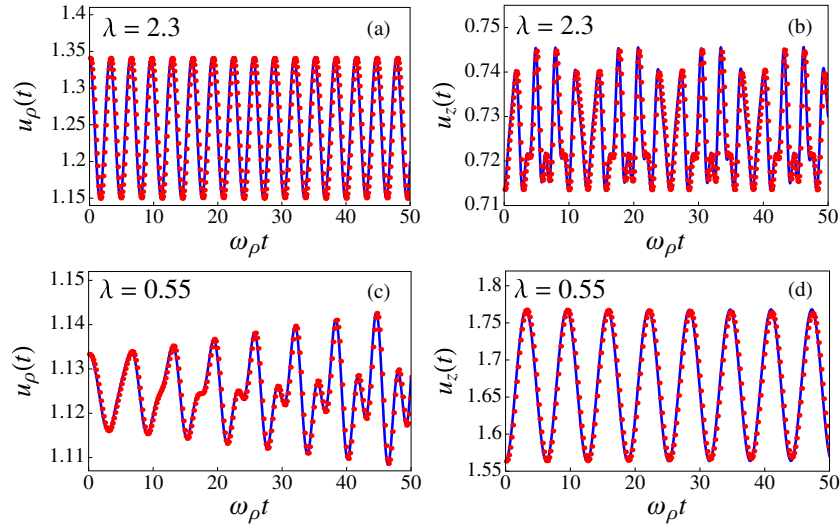


Figure 5. A comparison of analytic (solid blue lines) and numeric (red dots) results for a BEC dynamics with a pure repulsive two-body interaction $p = 1$, $k = 0$ and $\varepsilon = 0.1$. The top panels show dynamics of (a) radial and (b) longitudinal condensate widths for the trap aspect ratio $\lambda = 2.3$ as a function of the dimensionless time $\omega_\rho t$; the bottom panels show dynamics of (c) radial and (d) longitudinal BEC widths for $\lambda = 0.55$.

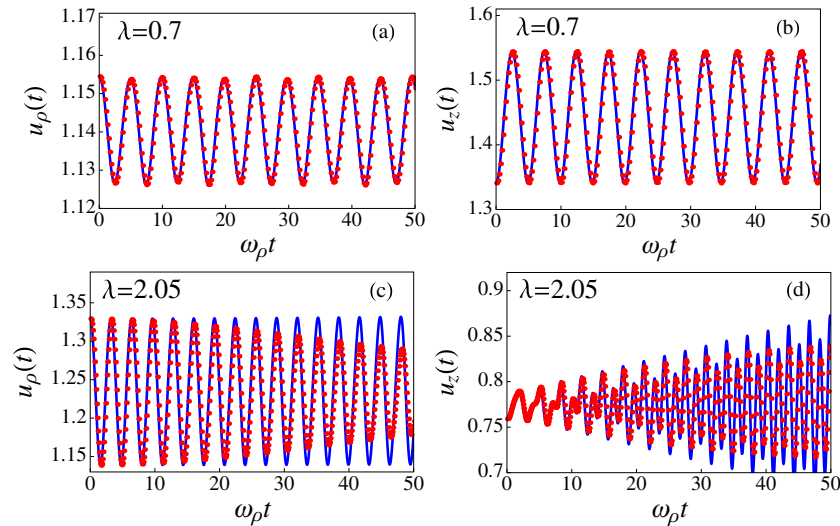


Figure 6. A comparison of analytic (solid blue lines) and numeric (red dots) results for BEC dynamics for a repulsive two-body interaction $p = 1$ and a repulsive three-body interaction $k = 0.001$, with $\varepsilon = 0.1$. The top panels show dynamics of (a) radial and (b) longitudinal condensate widths for the trap aspect ratio $\lambda = 0.7$ as a function of the dimensionless time $\omega_\rho t$; the bottom panels show dynamics of (c) radial and (d) longitudinal BEC widths for $\lambda = 2.05$.

these values of parameters, the relative shift in the quadrupole mode frequency is of the order of 0.3%, and therefore third-order perturbation theory yields a quite accurate description of the system dynamics. The same applies to the top panels of figure 6, where $\lambda = 0.7$ is far from any resonance. However, for $\lambda = 2.05$ (bottom panels), we observe some disagreement, which increases with propagation time. This is due to the fact that $p = 1$, $k = 0.001$, $\lambda = 2.05$ is close to a geometric resonance, as we will see in figure 8(b). In this case, the perturbatively calculated shift in the quadrupole mode frequency is much larger than that for the bottom panels of figure 5. For this reason, after a long enough time the third-order perturbation theory is not sufficiently accurate. Although it gives a qualitatively correct description of the behaviour of the system, one would have to go to higher orders in

perturbation theory to get more accurate agreement with the numerical results. Such a behaviour in the bottom panels of figure 6 is just a telltale of the occurrence of a geometric resonance, and a subsequent analysis of frequency shifts is the only proper way to identify these resonances in a more quantitative way.

However, before we present this analysis, we show in figure 7 the excitation spectra of the BEC dynamics which corresponds to the initial conditions (21) for $p = 1$, $k = 0.001$ and two values of the trap aspect ratio, $\lambda = 1.9$ and $\lambda = 0.5$. For the parameter values in figure 7(a), the linear stability analysis yields breathing and quadrupole mode frequencies (14) with $\omega_B = 3.65$ and $\omega_Q = 1.96$, while for the parameters in figure 7(b), we obtain $\omega_B = 2.01$ and $\omega_Q = 0.905$, all expressed in units of ω_ρ . In both graphs, we

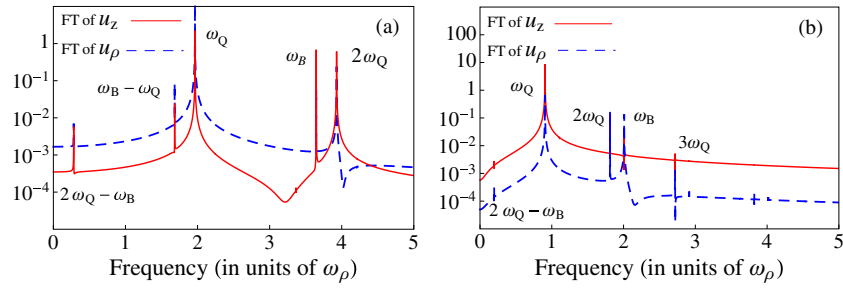


Figure 7. Fourier spectra of the BEC dynamics obtained by numerically solving the system of equations (7) and (8) for a repulsive two-body interaction $p = 1$, a repulsive three-body interaction $k = 0.001$, and $\varepsilon = 0.1$ for (a) $\lambda = 1.9$ and (b) $\lambda = 0.5$. Each graph shows spectra of both longitudinal and radial condensate widths. The locations of all peaks are identified as linear combinations of the quadrupole and the breathing mode frequencies, in correspondence with the analysis based on the developed perturbation theory.

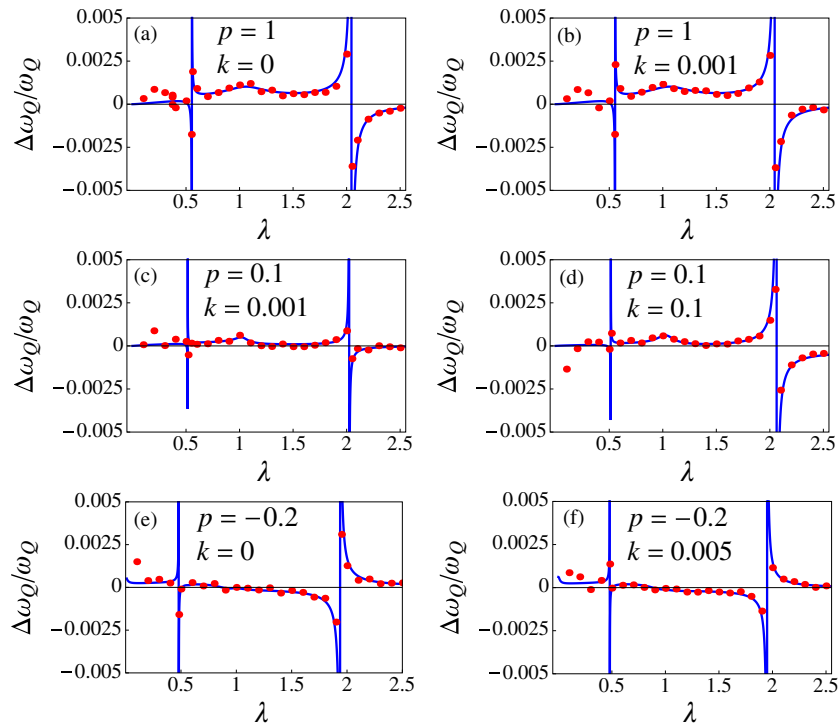


Figure 8. Relative frequency shift of the quadrupole mode as a function of the trap aspect ratio λ for $\varepsilon = 0.1$ and different values of two-body and three-body interaction strengths: (a) $p = 1, k = 0$, (b) $p = 1, k = 0.001$, (c) $p = 0.1, k = 0.001$, (d) $p = 0.1, k = 0.1$, (e) $p = -0.2, k = 0$, (f) $p = -0.2, k = 0.005$. The solid lines represent the analytical result (32), while dots are obtained by a numerical analysis of the corresponding excitation spectrum for each value of λ , as described in figure 7.

can see that the Fourier spectra contain two basic modes, ω_Q and ω_B , whose values agree well with those obtained from the linear stability analysis in equation (14), and a multitude of higher order harmonics, which are linear combinations of the two modes, as pointed out in subsection 4.1.

Now we compare the derived analytical results for the frequency shifts of the quadrupole and the breathing modes with the results of numerical simulations for the BEC systems with two- and three-body contact interactions in a cylindrical trap. In particular, we note that the calculated frequency shifts close to geometric resonances reveal poles, which are an artefact of the perturbative approach. Indeed, our detailed numerical calculations show that the observed frequencies remain finite through the whole geometric resonance. In figures 8 and 9, we present the comparison of analytic (solid lines) and numeric (dots) values of relative frequency shifts as

functions of the trap aspect ratio λ . The analytical results are calculated from equations (32) and (35), respectively, while the numerical data are obtained from a Fourier analysis of the excitation spectrum, i.e. for each value of λ we have calculated the corresponding Fourier spectra, as in figure 7, and then extracted the frequency values of the quadrupole and the breathing mode.

In figure 8(a), we show a special case of a pure two-body interaction, when $k = 0$. The condition for a geometric resonance $\omega_B = 2\omega_Q$ yields the trap aspect ratios $\lambda_1 = 0.555$ and $\lambda_2 = 2.056$, which is in good agreement with the numerical data, as we can see from the graph. The existence of a geometric resonance at $\lambda_1 = 0.555$ is responsible for a violent dynamics seen in the bottom panels of figure 5, as we have pointed out earlier. However, by analysing the frequency shifts we can conclusively show that, indeed, the geometric

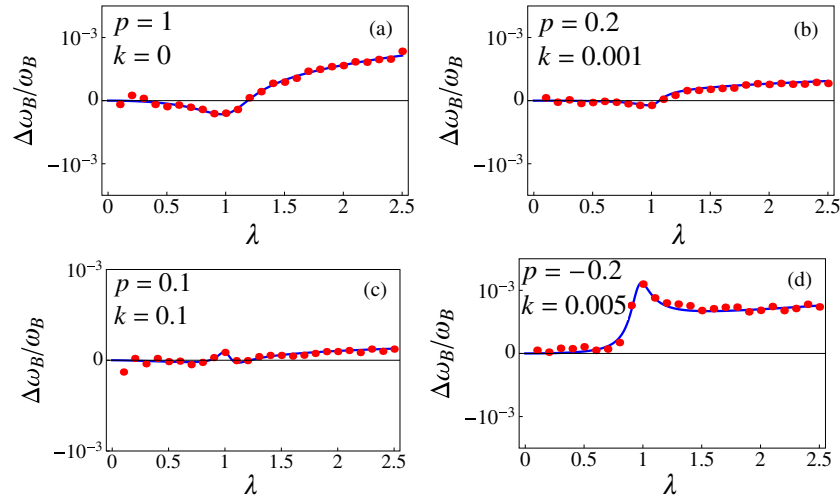


Figure 9. Relative frequency shift of the breathing mode as a function of the trap aspect ratio λ for $\varepsilon = 0.1$ and different values of two-body and three-body interaction strengths: (a) $p = 1, k = 0$, (b) $p = 0.2, k = 0.001$, (c) $p = 0.1, k = 0.1$, (d) $p = -0.2, k = 0.005$. The solid lines represent the analytical result (35), while dots are obtained by a numerical analysis of the corresponding excitation spectrum for each value of λ , as described in figure 7.

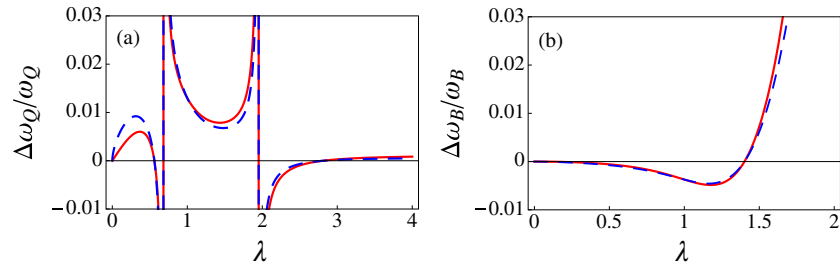


Figure 10. Comparison of the analytical results for the relative frequency shifts of (a) quadrupole and (b) breathing modes in the Thomas–Fermi limit from [18] derived using the parabolic variational ansatz (solid red lines) and the analytical results derived here using the Poincaré–Lindstedt perturbation theory with the Gaussian variational ansatz (dashed blue lines).

resonance is present. In further graphs, we see that the excellent agreement between analytical and numerical results also holds for other values of p and k , including the case of an attractive two-body interaction $p = -0.2$, which is still within the BEC stability region. It is interesting to note the observation that the asymptotic approach to geometric resonances for the case of an attractive two-body interaction is reversed compared to the case of a repulsive two-body interaction. For instance, we can see in figure 8(d) that $\Delta\omega_Q/\omega_Q \rightarrow \infty$ when $\lambda \rightarrow \lambda_2^-$, and $\Delta\omega_Q/\omega_Q \rightarrow -\infty$ when $\lambda \rightarrow \lambda_2^+$, while for an attractive $p = -0.2$ in figure 8(f) we see that the situation is reversed.

In figure 9, we compare analytic and numeric results for a frequency shift of the breathing mode. As for the quadrupole mode, the agreement is excellent for both repulsive and attractive two-body interactions. As pointed out in subsection 4.2, there are no geometric resonances for the breathing mode frequency, since the corresponding condition $\omega_Q = 2\omega_B$ cannot be satisfied.

Finally, we compare our derived analytic results with those from [18], where frequency shifts of collective modes were calculated in the Thomas–Fermi (TF) limit using a hydrodynamic approach. In terms of our variational approach, the TF limit corresponds to the limit $p \rightarrow \infty$, so that

equation (14) for the frequencies of the breathing and the quadrupole mode reduces to

$$\omega_{B,Q}^2 = 2 + \frac{3}{2}\lambda^2 \pm \frac{1}{2}\sqrt{16 - 16\lambda^2 + 9\lambda^4}, \quad (36)$$

which is in agreement with [18]. The condition for a geometric resonance $\omega_B = 2\omega_Q$ thus yields trap aspect ratios $\lambda_{1,2} = (\sqrt{125} \pm \sqrt{29})/\sqrt{72}$, i.e. $\lambda_1 \approx 0.683$ and $\lambda_2 \approx 1.952$.

Figure 10 gives a comparison of the relative frequency shifts in the TF limit calculated in [18] using a hydrodynamic approach, and our analytical results obtained using the Poincaré–Lindstedt perturbation theory. Despite the good agreement, we observe small differences, which are due to the fact that [18] uses a parabolic variational ansatz for the condensate wavefunction, while we use the Gaussian ansatz in equation (3). We have confirmed that, when applied to the parabolic variational ansatz, our perturbative approach yields frequency shifts in perfect agreement with [18].

5. Resonant mode coupling

In this section, we study the phenomenon of nonlinearity-induced resonant mode coupling. As already pointed out, even if a BEC system is excited precisely along the quadrupole or, equivalently, the breathing mode, the emerging dynamics

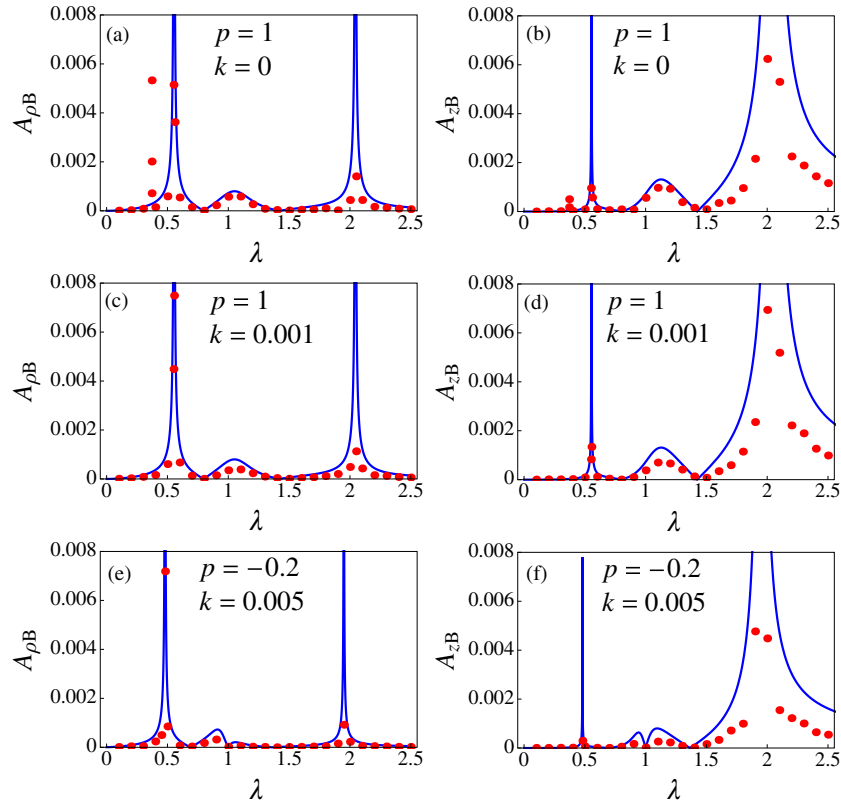


Figure 11. Amplitudes of the breathing mode emerging in the second order of the perturbation theory from BEC dynamics after initially only the quadrupole mode is excited, given as functions of the trap aspect ratio λ for $\varepsilon = 0.1$ and different values of two-body and three-body interaction strengths p and k . The amplitudes $A_{\rho B}$ and A_{zB} from equations (40) and (41) correspond to the radial and the longitudinal condensate widths of the emerging breathing mode dynamics.

will lead to small oscillations which initially involve only the corresponding mode, but then the other collective mode will eventually step in, as well as higher harmonics of the two modes and their linear combinations will appear. If the trap confinement of the system allows a geometric resonance, this could greatly enhance the mode coupling and speed up the emergence of those modes which are initially not excited, and therefore we designate it as a resonant mode coupling. We focus on the experimentally most studied case of a repulsive two-body interaction, although all derived analytical results are also valid for the case of an attractive interaction. As effects of three-body interactions are usually small, and their main contribution is related to a stabilization/destabilization of the condensate, we focus on the emergence of a resonant mode coupling due to geometric resonances.

To demonstrate this phenomenon, we use the perturbative solution of equations (7) and (8) with the initial conditions defined by equations (21), for which the initial state coincides with the equilibrium with a small perturbation proportional to the quadrupole mode eigenvector. The second-order perturbative solution can then be written as

$$\mathbf{u}_0 + \begin{pmatrix} A_{\rho Q} \\ A_{zQ} \end{pmatrix} \cos \omega_Q t + \begin{pmatrix} A_{\rho B} \\ A_{zB} \end{pmatrix} \cos \omega_B t + \dots, \quad (37)$$

where dots represent higher harmonics and the respective amplitudes are given by

$$A_{\rho Q} = \varepsilon u_{\rho Q} + \varepsilon^2 \mathcal{A}_{\rho Q2} \frac{u_{\rho Q}^2}{\omega_Q^2}, \quad (38)$$

$$A_{zQ} = c_1 A_{\rho Q}, \quad (39)$$

$$A_{\rho B} = \varepsilon^2 \mathcal{A}_{\rho B2} \frac{u_{\rho Q}^2 (\omega_B^2 - 2\omega_Q^2)}{\omega_B^2 (\omega_B^2 - 4\omega_Q^2)}, \quad (40)$$

$$A_{zB} = c_2 A_{\rho B}. \quad (41)$$

Note that the absence of terms linear in ε in expressions for $A_{\rho B}$ and A_{zB} is due to the initial condition, i.e. the fact that, initially, we only excite the quadrupole mode. The constants $c_{1,2}$ in the above expressions are defined by equation (26), while $\mathcal{A}_{\rho Q2}$ and $\mathcal{A}_{\rho B2}$ are calculated to be

$$\mathcal{A}_{\rho Q2} = \frac{c_2 \gamma_\rho + c_1 c_2 \alpha + c_1^2 c_2 \beta - \alpha - 4c_1 \beta - c_1^2 \gamma_z}{3(c_1 - c_2)}, \quad (42)$$

$$\mathcal{A}_{\rho B2} = \frac{-c_1^3 \beta + \alpha - c_1 \gamma_\rho + 4c_1 \beta - c_1^2 \alpha + c_1^2 \gamma_z}{c_1 - c_2}, \quad (43)$$

with $\alpha, \beta, \gamma_\rho, \gamma_z$ defined as

$$\alpha = \frac{3p}{u_{\rho 0}^4 u_{z 0}^2} + \frac{10k}{u_{\rho 0}^6 u_{z 0}^3}, \quad \beta = \frac{p}{u_{\rho 0}^3 u_{z 0}^3} + \frac{3k}{u_{\rho 0}^5 u_{z 0}^4}, \quad (44)$$

$$\gamma_\rho = \frac{6}{u_{\rho 0}^5} + \frac{6p}{u_{\rho 0}^5 u_{z 0}} + \frac{15k}{u_{\rho 0}^7 u_{z 0}^2}, \quad \gamma_z = \frac{6}{u_{z 0}^5} + \frac{3p}{u_{\rho 0}^2 u_{z 0}^4} + \frac{6k}{u_{\rho 0}^4 u_{z 0}^5} \quad (45)$$

In figure 11, we see the comparison of the derived analytical results, which emerge in the second order, and

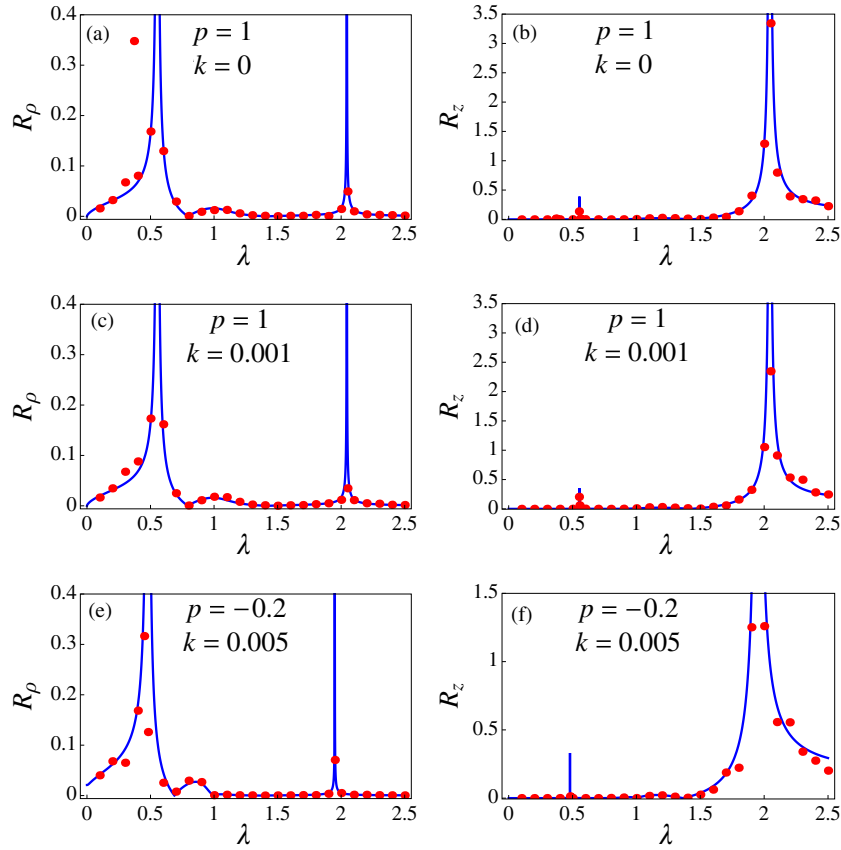


Figure 12. Ratios of breathing and quadrupole mode amplitudes emerging in the second order of the perturbation theory after initially only the quadrupole mode is excited, given as functions of the trap aspect ratio λ for $\varepsilon = 0.1$ and different values of two-body and three-body interaction strengths p and k . The quantities R_ρ and R_z from equations (46) and (47) correspond to ratios of amplitudes of the breathing and the quadrupole mode in the radial and longitudinal condensate widths.

corresponding numerical simulations for the amplitudes of the breathing mode. The numerical results are obtained, as before, by extracting the amplitude of the breathing mode from the Fourier excitation spectra of the system for each value of the trap aspect ratio λ . The agreement is quite good, and we see again a resonant behaviour, which occurs at the same trap aspect ratios as for the frequency shift of the quadrupole mode. From equations (40) and (41), we actually see that the resonances occur when the condition $\omega_B = 2\omega_Q$ is satisfied, which is precisely the same condition as for the frequency shift. This is not surprising, since amplitudes are expressed in terms of frequencies of the collective modes, and a resonant behaviour of the quadrupole mode frequency leads to resonances in the amplitudes for the same values of λ . Therefore, geometric resonances are not only reflected in the resonances of frequency shifts of collective modes, but also in the resonant mode coupling.

In addition to the absolute values of the breathing mode amplitudes, which are excited through the resonant mode coupling, it is also interesting to look at their relative values, compared to the quadrupole mode amplitudes, i.e.

$$R_\rho = \frac{A_{\rho B}}{A_{\rho Q}} \propto \frac{\omega_B^2 - 2\omega_Q^2}{\omega_B^2 - 4\omega_Q^2}, \quad (46)$$

$$R_z = \frac{A_{zB}}{A_{zQ}} \propto \frac{\omega_B^2 - 2\omega_Q^2}{\omega_B^2 - 4\omega_Q^2}. \quad (47)$$

Figure 12 shows the comparison of analytical and numerical results for the relative ratio of amplitudes of the resonance-excited breathing mode. Due to the geometric resonances, we see that the trap aspect ratio can be tuned in such a way that the resonant mode coupling excites the breathing mode with an amplitude far larger than that of the quadrupole mode, which serves as the source of excitation.

Furthermore, from equations (40) and (41) we see that, if the geometry of the trap is tuned such that $\omega_B = \omega_Q\sqrt{2}$, then the amplitudes of the breathing mode vanish simultaneously, i.e. $A_{\rho B} = A_{zB} = 0$. Although this is true only in the second-order perturbation theory, it still represents a condition for a significant suppression of the resonant mode coupling. Therefore, the tunability of the trap aspect ratio offers a unique tool for enhancing and suppressing the mode coupling in a BEC, which might be of broad experimental interest.

In a similar way, we can initially excite only the breathing mode, which corresponds to equations (7) and (8) with initial conditions defined in equations (33). The solution in the second-order perturbation theory has again the form

$$\mathbf{u}_0 + \begin{pmatrix} A_{\rho B} \\ A_{zB} \end{pmatrix} \cos \omega_B t + \begin{pmatrix} A_{\rho Q} \\ A_{zQ} \end{pmatrix} \cos \omega_Q t + \dots, \quad (48)$$

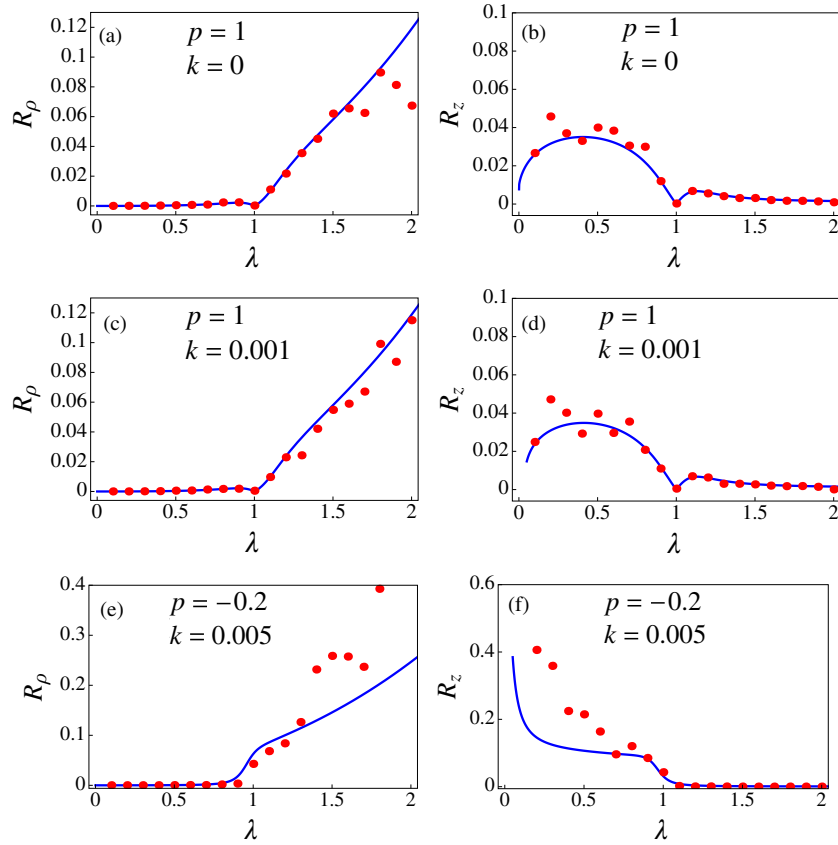


Figure 13. Ratios of quadrupole and breathing mode amplitudes emerging in the second order of the perturbation theory after initially only the breathing mode is excited, given as functions of the trap aspect ratio λ for $\varepsilon = 0.1$ and different values of two-body and three-body interaction strengths p and k . The quantities R_ρ and R_z from equations (55) and (56) correspond to ratios of amplitudes of the breathing and the quadrupole modes in the radial and longitudinal condensate widths.

but now the respective amplitudes read

$$A_{\rho B} = \varepsilon u_{\rho B} + \varepsilon^2 \mathcal{A}_{\rho B2} \frac{u_{\rho B}^2}{\omega_B^2}, \quad (49)$$

$$A_{zB} = c_2 A_{\rho B}, \quad (50)$$

$$A_{\rho Q} = \varepsilon^2 \mathcal{A}_{\rho Q2} \frac{u_{\rho B}^2 (2\omega_B^2 - \omega_Q^2)}{\omega_Q^2 (4\omega_B^2 - \omega_Q^2)}, \quad (51)$$

$$A_{zQ} = c_1 A_{\rho Q}, \quad (52)$$

and the coefficients $\mathcal{A}_{\rho B2}$ and $\mathcal{A}_{\rho Q2}$ are given by

$$\mathcal{A}_{\rho B2} = \frac{-c_1 \gamma_\rho - c_1 c_2 \alpha - c_1 c_2^2 \beta + \alpha + 4c_2 \beta + c_2^2 \gamma_z}{3(c_1 - c_2)}, \quad (53)$$

$$\mathcal{A}_{\rho Q2} = \frac{c_2^3 \beta - \alpha + c_2 \gamma_\rho - 4c_2 \beta + c_2^2 \alpha - c_2^2 \gamma_z}{c_1 - c_2}. \quad (54)$$

In this case, the ratios of amplitudes are given by

$$R_\rho = \frac{A_{\rho Q}}{A_{\rho B}} \propto \frac{2\omega_B^2 - \omega_Q^2}{4\omega_B^2 - \omega_Q^2}, \quad (55)$$

$$R_z = \frac{A_{zQ}}{A_{zB}} \propto \frac{2\omega_B^2 - \omega_Q^2}{4\omega_B^2 - \omega_Q^2}. \quad (56)$$

Figure 13 compares analytical and numerical results for the mode coupling when initially only the breathing mode is excited, and then the quadrupole mode emerges due to the mode coupling. As for the case of the breathing mode frequency shift, there are no resonances, since $\omega_B > \omega_Q$, and the resonance condition $2\omega_B = \omega_Q$ cannot be satisfied, as is confirmed by the graphs. Therefore, the amplitudes do not experience resonances in this case, contrary to what we have observed in figure 12. Again, this can be explained by the fact that amplitudes are functions of the breathing mode frequency, which does not experience any resonances, and hence the same is valid for the corresponding amplitude. Also, the condition $\omega_B \sqrt{2} = \omega_Q$ cannot be satisfied, and therefore the amplitude of the quadrupole mode cannot be fully suppressed here, contrary to the case presented in figure 12. For a repulsive two-body interaction in figures 13(a)–(d), we see that the ratios R_ρ and R_z are below 10%, and the mode coupling mechanism is not able to produce a significant amplitude for the quadrupole mode. For the case of an attractive two-body interaction in figures 13(e)–(f), the ratio increases and the generated quadrupole mode amplitude is stronger. Here the agreement between analytical and numerical results is only qualitative, so that the perturbation theory would have to be carried out to higher orders in the small parameter ε in order to improve the agreement.

6. Conclusions

We have studied the dynamics and collective excitations of a BEC for different trap aspect ratios at zero temperature. In particular, we have investigated prominent resonant effects that arise due to two- and three-body interactions, and their delicate interplay. We have discussed the stability of a condensate in an axially symmetric harmonic trap for the experimentally most relevant setups: repulsive and attractive two-body interactions, attractive two-body and repulsive three-body interactions, and attractive two- and three-body interactions. We have shown that even a small repulsive three-body interaction is able to extend the stability region of the condensate beyond the critical number of atoms when the two-body interaction is attractive.

Using a perturbation theory and a Poincaré–Lindstedt analysis of a Gaussian variational approach for the condensate wavefunction, we have studied in detail the relation between resonant effects due to two- and three-body interactions, and the effects of the trap geometry. Within the variational approach and the Poincaré–Lindstedt method, we have analytically calculated frequency shifts and a mode coupling in order to identify geometric resonances of collective oscillation modes of an axially symmetric BEC. We have also shown that the observed geometric resonances can be suppressed if two- and three-body interactions are appropriately fine-tuned.

To verify the derived analytical results, we have used numerical simulations, which provide detailed excitation spectra of the BEC dynamics. We have numerically observed and analytically described several prominent nonlinear features of BEC systems: significant shifts in the frequencies of collective modes, generation of higher harmonics and linear combinations of collective modes, as well as resonant and non-resonant mode coupling. We have shown that, even if the system is excited so that the perturbation corresponds initially to the eigenvector of a particular mode, the nonlinear dynamics of the condensate will eventually excite also other modes due to the mode coupling. The presence of geometric resonances can significantly enhance this effect, as we have shown using the developed perturbation theory. All obtained analytical results are found to be in good agreement with the numerical results. Furthermore, the results for frequency shifts are shown to coincide with the earlier derived analytical results [18] within the hydrodynamic approach in the Thomas–Fermi approximation. In future work, we plan to extend the present analysis and also include the effects of quantum fluctuations [106].

Acknowledgments

This work was supported in part by the Ministry of Education, Science, and Technological Development of the Republic of Serbia under projects no. ON171017, NAD-BEC and NAI-DBEC, by DAAD—German Academic and Exchange Service under projects NAD-BEC and NAI-DBEC, and by the European Commission under EU FP7 projects PRACE-1IP, PRACE-2IP, PRACE-3IP, HP-SEE and EGI-InSPIRE. Both AB and AP gratefully acknowledge a fellowship from the Hanse–Wissenschaftskolleg.

References

- [1] Anderson M H, Ensher J R, Matthews M R, Wieman C E and Cornell E A 1995 *Science* **269** 198
- [2] Davis K B, Mewes M-O, Andrews M R, van Druten N J, Durfee D S, Kurn D M and Ketterle W 1995 *Phys. Rev. Lett.* **75** 3969
- [3] Bradley C C, Sackett C A and Hulet R G 1997 *Phys. Rev. Lett.* **78** 985
- [4] Gerton J M, Strelak D, Prodan I and Hulet R G 2000 *Nature* **408** 692
- [5] Cornish S L, Claussen N R, Roberts J L, Cornell E A and Wieman C E 2000 *Phys. Rev. Lett.* **85** 1795
- [6] Roberts J L, Claussen N R, Cornish S L, Donley E A, Cornell E A and Wieman C E 2001 *Phys. Rev. Lett.* **86** 4211
- [7] Jin D S, Ensher J R, Matthews M R, Wieman C E and Cornell E A 1996 *Phys. Rev. Lett.* **77** 420
- [8] Mewes M-O, Andrews M R, van Druten N J, Kurn D M, Durfee D S, Townsend C G and Ketterle W 1996 *Phys. Rev. Lett.* **77** 988
- [9] Stamper-Kurn D M, Miesner H-J, Inouye S, Andrews M R and Ketterle W 1998 *Phys. Rev. Lett.* **81** 500
- [10] Yang L, Wang X-R, Li K, Tan X-Z, Xiong H-W and Lu B-L 2009 *Chin. Phys. Lett.* **26** 076701
- [11] Stringari S 1996 *Phys. Rev. Lett.* **77** 2360
- [12] Edwards M, Ruprecht P A, Burnett K, Dodd R J and Clark C W 1996 *Phys. Rev. Lett.* **77** 1671
- [13] Edwards M, Dodd R J, Clark C W and Burnett K 1996 *J. Res. Natl Inst. Stand. Technol.* **101** 553
- [14] Singh K G and Rokhsar D S 1996 *Phys. Rev. Lett.* **77** 1667
- [15] Pérez-García V M, Michinel H, Cirac J I, Lewenstein M and Zoller P 1996 *Phys. Rev. Lett.* **77** 5320
- [16] Pérez-García V M, Michinel H, Cirac J I, Lewenstein M and Zoller P 1997 *Phys. Rev. A* **56** 1424
- [17] You L, Hoston W and Lewenstein M 1997 *Phys. Rev. A* **55** R1581
- [18] Dalfovo F, Minniti C and Pitaevskii L 1997 *Phys. Rev. A* **56** 4855
- [19] Vidanović I, Balaž A, Al-Jibbouri H and Pelster A 2011 *Phys. Rev. A* **84** 013618
- [20] Hechenblaikner G, Maragò O M, Hodby E, Arlt J, Hopkins S and Foot C J 2000 *Phys. Rev. Lett.* **85** 692
- [21] Hechenblaikner G, Morgan S A, Hodby E, Maragò O M and Foot C J 2002 *Phys. Rev. A* **65** 033612
- [22] Pitaevskii L and Stringari S 1997 *Phys. Lett. A* **235** 398
- [23] Lee C, Huang J, Deng H, Dai H and Xu J 2012 *Front. Phys.* **7** 109
- [24] Pitaevskii L 1997 *Phys. Lett. A* **229** 406
- [25] Graham R, Walls D F and Collett M J 1998 *Phys. Rev. A* **57** 503
- [26] Castin Y and Dum R 1996 *Phys. Rev. Lett.* **77** 5315
- [27] García-Ripoll J J, Pérez-García V M and Torres P 1999 *Phys. Rev. Lett.* **83** 1715
- [28] García-Ripoll J J and Pérez-García V M 1999 *Phys. Rev. A* **59** 2220
- [29] Engels P, Atherton C and Hofer M A 2007 *Phys. Rev. Lett.* **98** 095301
- [30] Nicolin A I, Carretero-González R and Kevrekidis P G 2007 *Phys. Rev. A* **76** 063609
- [31] Pollack S E, Dries D, Junker M, Chen Y P, Corcovilos T A and Hulet R G 2009 *Phys. Rev. Lett.* **102** 090402
- [32] Nicolin A I 2011 *Phys. Rev. E* **84** 056202
- [33] Hamner C, Chang J J, Engels P and Hofer M A 2011 *Phys. Rev. Lett.* **106** 065302
- [34] Nicolin A I 2011 *Rom. Rep. Phys.* **63** 1329
- [35] Middelkamp S, Chang J J, Hamner C, Carretero-González R, Kevrekidis P G, Achilleos V, Frantzeskakis D J, Schmelcher P and Engels P 2011 *Phys. Lett. A* **375** 642
- [36] Nicolin A I 2012 *Physica A* **391** 1062

- [37] Balaž A and Nicolini A I 2012 *Phys. Rev. A* **85** 023613
- [38] Kobayakov D, Bychkov V, Lundh E, Bezett A and Marklund M 2012 *Phys. Rev. A* **86** 023614
- [39] Pepe F V, Facchi P, Florio G and Pascazio S 2012 *Phys. Rev. A* **86** 023629
- [40] Gaul C, Lima R P A, Diaz E, Müller C A and Dominguez-Adame F 2009 *Phys. Rev. Lett.* **102** 255303
- [41] Pollack S E, Dries D, Hulet R G, Magalhães K M F, Henn E A L, Ramos E R F, Caracanhas M A and Bagnato V S 2010 *Phys. Rev. A* **81** 053627
- [42] Sabari S, Raja R V J, Porsezian K and Muruganandam P 2010 *J. Phys. B: At. Mol. Opt. Phys.* **43** 125302
- [43] Gaul C, Diaz E, Lima R P A, Dominguez-Adame F and Müller C A 2011 *Phys. Rev. A* **84** 053627
- [44] Vidanović I, Al-Jibbouri H, Balaž A and Pelster A 2012 *Phys. Scr. T* **149** 014003
- [45] Hodby E, Maragò O M, Hechenblaikner G and Foot C J 2001 *Phys. Rev. Lett.* **86** 2196
- [46] Kasamatsu K, Tsubota M and Ueda M 2004 *Phys. Rev. A* **69** 043621
- [47] Ramos E R F, dos Santos F E A, Caracanhas M A and Bagnato V S 2012 *Phys. Rev. A* **85** 033608
- [48] Dalfovo F, Minniti C, Stringari S and Pitaevskii L 1997 *Phys. Lett. A* **227** 259
- [49] Leanhardt A E, Chikkatur A P, Kielpinski D, Shin Y, Gustavson T L, Ketterle W and Pritchard D E 2002 *Phys. Rev. Lett.* **89** 040401
- [50] Zhang W, Wright E M, Pu H and Meystre P 2003 *Phys. Rev. A* **68** 023605
- [51] Zhang A-X and Xue J-K 2007 *Phys. Rev. A* **75** 013624
- [52] Köhler T 2002 *Phys. Rev. Lett.* **89** 210404
- [53] Tolra B L, O'Hara K M, Huckans J H, Phillips W D, Rolston S L and Porto J V 2004 *Phys. Rev. Lett.* **92** 190401
- [54] Ruprecht P A, Holland M J, Burnett K and Edwards M 1995 *Phys. Rev. A* **51** 4704
- [55] Akhmediev N, Das M P and Vagov A V 1999 *Int. J. Mod. Phys. B* **13** 625
- [56] Gammal A, Frederico T, Tomio L and Chomaz Ph 2000 *J. Phys. B: At. Mol. Opt. Phys.* **33** 4053
- [57] Tomio L, Filho V S, Gammal A and Frederico T 2003 *Laser Phys.* **13** 582
- [58] Abdullaev F K, Gammal A, Tomio L and Frederico T 2001 *Phys. Rev. A* **63** 043604
- [59] Tewari S P, Silotia P, Saxena A and Gupta L K 2006 *Phys. Lett. A* **359** 658
- [60] Wamba E, Mohamadou A and Kofane T C 2008 *J. Phys. B: At. Mol. Opt. Phys.* **41** 225403
- [61] Abdullaev F K and Salerno M 2005 *Phys. Rev. A* **72** 033617
- [62] Chen B-L, Huang X-B, Kou S-P and Zhang Y 2008 *Phys. Rev. A* **78** 043603
- [63] Chen Y, Zhang K-Z and Chen Y 2009 *J. Phys. B: At. Mol. Opt. Phys.* **42** 185302
- [64] Zhou K, Liang Z and Zhang Z 2010 *Phys. Rev. A* **82** 013634
- [65] Silva-Valencia J and Souza A M C 2011 *Phys. Rev. A* **84** 065601
- [66] Sowiński T 2012 *Phys. Rev. A* **85** 065601
- [67] Singh M, Dhar A, Mishra T, Pai R V and Das B P 2012 *Phys. Rev. A* **85** 051604
- [68] Safavi-Naini A, von Stecher J, Capogrosso-Sansone B and Rittenhouse S T 2012 *Phys. Rev. Lett.* **109** 135302
- [69] Dasgupta R 2010 *Phys. Rev. A* **82** 063607
- [70] Roy U, Atre R, Sudheesh C, Kumar C N and Panigrahi P K 2010 *J. Phys. B: At. Mol. Opt. Phys.* **43** 025003
- [71] Ma J, Li Z and Xue J-K 2009 *Chin. Phys. B* **18** 4122
- [72] Josserand C, Pomeau Y and Rica S 1995 *Phys. Rev. Lett.* **75** 3150
- [73] Josserand C and Rica S 1997 *Phys. Rev. Lett.* **78** 1215
- [74] Berloff N G 2009 *Fluid Dyn. Res.* **41** 051403
- [75] Li H-C, Chen H-J and Xue J-K 2010 *Chin. Phys. Lett.* **27** 030304
- [76] Yong W-M, Wei X-F, Zhou X-Y and Xue J-K 2009 *Commun. Theor. Phys.* **51** 433
- [77] Peng P and Li G-Q 2009 *Chin. Phys. B* **18** 3221
- [78] Gross E P 1961 *Nuovo Cimento* **20** 454
- [79] Pitaevskii L P 1961 *Sov. Phys.—JETP* **13** 451
- [80] Pitaevskii L and Stringari S 2004 *Bose–Einstein Condensation* (Oxford: Clarendon)
- [81] Pethick C J and Smith H 2008 *Bose–Einstein Condensation in Dilute Gases* 2nd edn (Cambridge: Cambridge University Press)
- [82] Dalfovo F, Giorgini S, Pitaevskii L P and Stringari S 1999 *Rev. Mod. Phys.* **71** 463
- [83] Altin P A, Dennis G R, McDonald G D, Döring D, Debs J E, Close J D, Savage C M and Robins N P 2011 *Phys. Rev. A* **84** 033632
- [84] Efimov V 1971 *Sov. J. Nucl. Phys.* **12** 589
- [85] Efimov V 1979 *Sov. J. Nucl. Phys.* **29** 546
- [86] Braaten E and Nieto A 1999 *Eur. Phys. J. B* **11** 143
- [87] Gammal A, Frederico T and Tomio L 2001 *Phys. Rev. A* **64** 055602
- [88] Bulgac A 2002 *Phys. Rev. Lett.* **89** 050402
- [89] Trombettoni A and Smerzi A 2001 *Phys. Rev. Lett.* **86** 2353
- [90] Grimm R 2010 *Rev. Mod. Phys.* **82** 1225
- [91] Borzov D, Mashayekhi M S, Zhang S, Song J-L and Zhou F 2012 *Phys. Rev. A* **85** 023620
- [92] Bogoliubov N N and Mitropolsky Yu A 1961 *Asymptotic Methods in the Theory of Non-Linear Oscillations* (New York: Gordon and Breach)
- [93] Pelster A, Kleinert H and Schanz M 2003 *Phys. Rev. E* **67** 016604
- [94] Mickens R 1981 *An Introduction to Nonlinear Oscillations* (Cambridge: Cambridge University Press)
- [95] Minorsky N 1962 *Nonlinear Oscillations* (Princeton, NJ: Van Nostrand-Reinhold)
- [96] *Mathematica* symbolic calculation software package. Available at www.wolfram.com/mathematica
- [97] Muruganandam P and Adhikari S K 2009 *Comput. Phys. Commun.* **180** 1888
- [98] Vudragović D, Vidanović I, Balaž A, Muruganandam P and Adhikari S K 2012 *Comput. Phys. Commun.* **183** 2021
- [99] Vidanović I, Bogojević A, Balaž A and Belić A 2009 *Phys. Rev. E* **80** 066706
- [100] Balaž A, Vidanović I, Bogojević A and Pelster A 2010 *Phys. Lett. A* **374** 1539
- [101] Balaž A, Vidanović A, Bogojević A, Belić A and Pelster A 2011 *J. Stat. Mech.* **P03004**
- [102] Balaž A, Vidanović A, Bogojević A, Belić A and Pelster A 2011 *J. Stat. Mech.* **P03005**
- [103] Diakonov F K, Kalozoumis P A, Karanikas A I, Manifavas N and Schmelcher P 2012 *Phys. Rev. A* **85** 062110
- [104] Hu W H, Jin L and Song Z 2012 Dynamics of one-dimensional tight-binding models with arbitrary time-dependent external homogeneous fields arXiv:1205.6999
- [105] Balaž A, Vidanović I, Stojiljković D, Vudragović D, Belić A and Bogojević A 2012 *Commun. Comput. Phys.* **11** 739
- [106] Lima A R P and Pelster A 2012 *Phys. Rev. A* **86** 063609